Pergamon

0045-7949(95)00110-7

Computers & Structures Vol. 58, No. 1, pp. 51–58, 1996

0045-7949/96 $9.50 + 0.00

AN ENGINEERING PENETRATION/PERFORATION MODEL OF HEMISPHERICAL NOSED RIGID CYLINDRICAL RODS INTO STRAIN-HARDENING TARGETS

Y. Wu† and **R. C. Batra**‡

†2812 Charter Blvd, 207, Troy, MI 48083, U.S.A.
‡Department of Engineering Science and Mechanics, Virginia Polytechnic Institute and State University, Blacksburg, VA 24061-0219, U.S.A.

(*Received* 29 *June* 1994)

Abstract—We propose a four-stage model of the penetration/perforation by hemispherical-nosed rigid cylindrical rods into targets whose materials exhibit strain-hardening effects. During each stage of the penetration process, a kinematically admissible velocity field involving one or more unknown parameters is assumed. These parameters are determined by minimizing the rate of plastic dissipation. From this velocity field, the incremental deformations of the target, the penetration depth, the resisting force acting on the penetrator and hence its deceleration are evaluated. We propose a criterion for the formation and ejection of the cylindrical plug in the target and use it to study problems involving the perforation of the target. Computed results for the exit speed of the penetrator and, when the targets are not perforated, of the penetration depth are found to match well with the corresponding test values.

1. INTRODUCTION

One way to analyze an impact problem is to seek a solution of the dynamic equations expressing the balance of mass, linear momentum and internal energy subject to suitable initial and boundary conditions. However, this technique, while furnishing details of the deformation fields in the penetrator and the target, is computationally very expensive. When one is interested in gross effects such as the penetration depth, exit speed of the rod impacting at normal incidence a metallic plate and the time history of the speed of the rod, then one can use an approximate method to obtain reliable solutions with considerably less computational resources. Ravid and Bodner [1] proposed a five-stage model for the perforation of viscoplastic plates by flat-ended rigid projectiles. In each stage of deformation, a kinematically admissible velocity field containing some unknown parameters is presumed. These parameters are determined by utilizing a modification of the upper bound theorem of plasticity to include dynamic effects.

Batra and Chen [2] considered steady-state axisymmetric deformations of a thick viscoplastic target being penetrated by a fast moving long rigid cylindrical rod with a hemispherical nose. They presumed a kinematically admissible velocity field and determined the values of unknown parameters in it, by minimizing the error in the satisfaction of the balance of linear momentum. The engineering models of Ravid and Bodner, and Batra and Chen consider two-dimensional deformations of the target and regard the penetrator as rigid. The earlier models proposed by Birkhoff *et al.* [3] and Pack and Evans [4] used either the Bernoulli equation or its modification to describe the hypervelocity impact and are one-dimensional. At ordnance speeds (0.5–2 km s^{-1}) the material strength becomes an important parameter. Allen and Rogers [5], Alekseevskii [6] and Tate [7, 8] have incorporated the flow strength as a resistive pressure in the modified Bernoulli equation. These resistive pressures are empirically determined quantities and the predicted results depend strongly upon the assumed values of these parameters.

Here we generalize the engineering model of Ravid and Bodner in two respects, namely, to hemispherical nosed penetrators and also to very thick targets for which the penetrator comes to rest without perforating the target. However, the model is simpler in the sense that the entire deformation process is divided into four stages. The first stage corresponds to the case when the penetration depth is less than or equal to the radius R_0 of the penetrator; the second stage to the case when the penetration depth is between R_0 and $2R_0$. The velocity field assumed during the third stage simulates the target deformations when there is no bulge formed at the rear surface. During the fourth and final stage, a cylindrical plug develops ahead of the projectile and is assumed to eject out of the target when the bulge radius reaches a preassigned value. Ideally, one should incorporate a failure criterion based on a material property such as the fracture toughness. However, the computation of any such property during the penetration process is nearly impossible. For a given projectile diameter, its length, mass density, impact speed, and mechanical properties, mass density and thickness of the target, we can determine the time-histories of the penetrator speed, its location, the resisting force acting on it, and also the time-history of the state of deformation of a target particle, the rear surface bulge and the plug shape. If the target is thin enough or the impact speed is large enough for the target to be perforated, the analysis gives the exit speed of the projectile and the plug. The computed values of the penetration depths for thick targets and the exit speed of the projectile for perforated targets are found to match very well with the experimental values.

2. FORMULATION OF THE PROBLEM

We study the penetration/perforation of a viscoplastic target by a fast moving rigid cylindrical rod impacting at normal incidence the flat surface of the target. We assume that the target is a prismatic body of uniform cross-section and undergoes axisymmetric deformations, and neglect the effect of body forces on the deformations of the target. Instead of attempting to solve the dynamic equations expressing the balance of mass and the balance of linear momentum subjected to suitable initial and boundary conditions, we follow Ravid and Bodner [1] and assume a kinematically admissible velocity field most appropriate for the dominant deformation mechanism prevailing at that time. The presumed velocity field also satisfies compatibility conditions at the interface between the deforming and undeforming regions. Since the penetrator is being taken as rigid, its action on the target is modeled by regarding the impact force it exerts on the target as an external force.

The dissipation work rate, $\dot{W}_t$, equals the sum of three terms, $\dot{W}_v$ the working necessary to deform the material plastically, $\dot{W}_s$ the working of forces at the interface between the deforming and the undeforming target regions, and $\dot{W}_f$ the working of frictional forces at the target/penetrator interface. For every value of time t during each stage of deformation, the undetermined parameter in the presumed velocity field is found by minimizing $\dot{W}_t$. As pointed out by Ravid and Bodner [1] who also minimized $\dot{W}_t$, this can be motivated on the basis of Martin's [9] theorem on acceleration fields which states that the rate of work of the inertial force based on an assumed acceleration field would be an upper bound on the actual one.

Neglecting infinitesimal elastic deformations, the total rate of work required to deform the material plastically is given by

$$\dot{W}_v = \int_{\Omega_n} \boldsymbol{\sigma}_{ij}\mathbf{D}_{ij}\,\mathrm{d}\Omega = (\sigma_y)_n \dot{\epsilon}_n^{\text{eff}}\Omega_n \tag{1}$$

where

$$\dot{\epsilon}_n^{\text{eff}} = (\sqrt{\tfrac{2}{3}}/\Omega_n)\left(\int_{\Omega_n} \mathbf{D}_{ij}\mathbf{D}_{ij}\,\mathrm{d}\Omega\right)^{1/2}, \tag{2}$$

is the average effective plastic strain-rate over the region Ω_n, $(\sigma_y)_n$ is the strain-dependent flow stress corresponding to the strain ϵ_n^{eff}, $\boldsymbol{\sigma}_{ij}$ is the Cauchy stress tensor and $\mathbf{D}_{ij}$ is the strain-rate tensor. Note that $(\sigma_y)_n$ is uniform throughout the region Ω_n and corresponds to the value of the average strain in the region Ω_n. The dependence of σ_y upon the effective strain is modeled as

$$\sigma_y = A + B(\epsilon^{\text{eff}})^n,$$
$$\epsilon_n^{\text{eff}} = \sum(\dot{\epsilon}_n^{\text{eff}})\,\Delta t, \tag{3}$$

where A is the yield stress for the target material in a quasistatic simple tension or compression test, B is the strain-hardening coefficient and n is the strain-hardening exponent. The work reported herein can easily be generalized to include the dependence of σ_y upon the average effective plastic strain-rate, and other forms of dependence of σ_y upon the effective plastic strain.

At the boundary, S_m, between different regions, the tangential velocity may be discontinuous. Hence the working, $\dot{W}_s$, of forces acting on S_m can be approximated by

$$\dot{W}_s = \sum_m \frac{1}{\sqrt{3}}(\sigma_y)_m \int_{S_m} |\Delta V_r|\,\mathrm{d}S_m, \tag{4}$$

where ΔV_r is the difference in the tangential velocity of material particles across S_m, and $(\sigma_y)_m$ equals the minimum value of the average flow stress for the regions adjoining S_m. The index m in eqn (4) ranges over all interfaces separating different regions.

The rate, $\dot{W}_f$, of work done by frictional forces at the target/penetrator interface is given by

$$\dot{W}_f = \frac{\mu}{\sqrt{3}}\bar{\sigma}_y \int_{S_f} |\Delta V_f|\,\mathrm{d}S \tag{5}$$

where μ is the coefficient of friction, $\bar{\sigma}_y$ is the average flow stress for material particles on S_f, and ΔV_f equals the difference in the tangential velocities of the abutting target and penetrator particles at the contact surface.

In order to delineate the relation between $\dot{W}_v$, $\dot{W}_s$, $\dot{W}_f$ and the conditions at the impact surface, we start with the balance of linear momentum for the target, *viz.*,

$$\rho_t \dot{v}_i = \boldsymbol{\sigma}_{ij,j}, \tag{6}$$

where ρ_t is the mass-density of a target particle, v_i its velocity in an inertial frame, a superimposed dot indicates the material time derivative, and a comma followed by index j signifies partial differentiation with respect to x_j. Taking the inner product of eqn (6) with v_i, integrating the result over the deforming target region, and using the divergence theorem, we arrive at

$$\int_S f_i v_i\,\mathrm{d}S = \int_\Omega \boldsymbol{\sigma}_{ij}\mathbf{D}_{ij}\,\mathrm{d}\Omega + \int_\Omega \rho_t v_i \dot{v}_i\,\mathrm{d}\Omega, \tag{7}$$

where $f_i = \sigma_{ij} n_j$ equals the surface tractions acting at a point on the bounding surface S of Ω.

Recalling that

$$\dot{v}_i = \frac{\partial v_i}{\partial t} + \frac{\partial v_i}{\partial x_j} v_j, \tag{8}$$

we have

$$\int_\Omega \rho_t \dot{v}_i v_i \,\mathrm{d}\Omega = \int_\Omega \rho_t v_i \frac{\partial v_i}{\partial t} \mathrm{d}\Omega + \int_\Omega \rho_t v_i \frac{\partial v_i}{\partial x_j} v_j \,\mathrm{d}\Omega, \tag{9}$$

$$= \dot{W}_\mathrm{d} + \dot{W}_k. \tag{10}$$

The working $\dot{W}_\mathrm{p}$ of inertia forces of the projectile of mass m_p moving with the instantaneous speed V_p can be written as

$$\dot{W}_\mathrm{p} = m_\mathrm{p} \dot{V}_\mathrm{p} V_\mathrm{p}. \tag{11}$$

Since $\dot{V}_\mathrm{p}$ and V_p are collinear and point in opposite directions, $\dot{W}_\mathrm{p}$ is negative. Thus

$$\int_S f_i v_i \,\mathrm{d}S = -\dot{W}_\mathrm{p} - \dot{W}_\mathrm{f} - \dot{W}_\mathrm{s}, \tag{12}$$

which when combined with eqns (7) and (1) gives

$$-\dot{W}_\mathrm{p} = \dot{W}_\mathrm{f} + \dot{W}_\mathrm{s} + \dot{W}_\mathrm{v} + \dot{W}_\mathrm{d} + \dot{W}_k = \dot{W}_t + \dot{W}_\mathrm{d} + \dot{W}_k. \tag{13}$$

Equation (13) is the energy-rate balance for the complete system.

3. ANALYSIS OF TARGET'S DEFORMATIONS

3.1. *Stage* 1. *Penetration depth less than or equal to the penetrator radius*

Upon impact the target material deforms and there is a small lip region formed. The finite element solution of such problems by Batra and Chen [10] and Chen and Batra [11] suggests that in the deforming region I of target (cf. Fig. 1), the velocity field in spherical coordinates (ρ, θ, ϕ) can be written as

$$v_\rho = V_\mathrm{p} \cos\theta \left[1 + \frac{\eta^3}{(\eta-1)^2}\left(-\frac{1}{\rho} + \frac{2}{\rho^2} - \frac{1}{\rho^3}\right)\right],$$

$$1 \leqslant \rho \leqslant \eta, \tag{13a}$$

$$v_\theta = V_\mathrm{p} \sin\theta \left[-1 + \frac{\eta^3}{(\eta-1)^2}\left(\frac{1}{2\rho} - \frac{1}{2\rho^3}\right)\right]. \tag{13b}$$

Here the radial coordinate ρ has been nondimensionalized by the penetrator radius R_0, V_p is the current axial speed of the penetrator and the parameter η is to be determined by minimizing the total dissipation rate. The velocity field given by eqn (13) satisfies the continuity of the normal component of velocity at the target–penetrator interface and also at the boundary between the deforming and undeforming target regions. We are not aware of any public domain publication that lists the experimentally determined velocity field in the deforming penetrator region. For the velocity field given by eqn (13), $\operatorname{div} \mathbf{v} = 0$ and hence the mass density of the target material stays unchanged. Using $2\mathbf{D} = \operatorname{grad}\mathbf{v} + (\operatorname{grad}\mathbf{v})^\mathrm{T}$, we can compute the components of the strain-rate tensor which when substituted in eqns (1) and (2) result in the following:

$$\dot{W}_\mathrm{v} = 2\pi R_0^3 V_\mathrm{p} (\sigma_y)_1 \frac{\sqrt{2}\,\eta^3}{\sqrt{3}(\eta-1)^2} \int_{\Omega_1}$$

$$\times [c(\rho) + a(\rho)\cos^2\theta]^{1/2} \sin\theta \,\mathrm{d}\theta \,\mathrm{d}\rho, \tag{14a}$$

where

$$c(\rho) = \frac{2}{\rho^2} - \frac{6}{\rho^3} + \frac{9}{2\rho^4}, \tag{14b}$$

$$a(\rho) = \frac{3}{2} - \frac{12}{\rho} + \frac{31}{\rho^2} - \frac{30}{\rho^3} + \frac{9}{\rho^4}. \tag{14c}$$

We note that the size of Ω_1 and therefore values of angles θ_1 and θ_2 in Fig. 1 vary with time t. Expressions for $\dot{W}_\mathrm{d}$, $\dot{W}_k$, $\dot{W}_\mathrm{f}$ etc. are given in the following subsection.

3.2. *Stage* 2. *Penetration depth between* $\mathbf{R}_0$ *and* $2\mathbf{R}_0$

This stage will develop shortly after initial impact and is characterized by continuously growing plastic zones surrounding the projectile. We presume that the deforming target region can be divided approximately into two distinct regions; region I which is undergoing severe plastic deformations and the material particles are moving both in the radial and

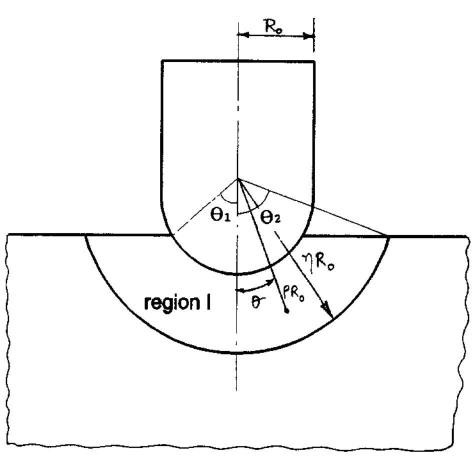

Fig. 1. A schematic sketch of the penetrator position and deforming target region during stage 1 of the penetration process.

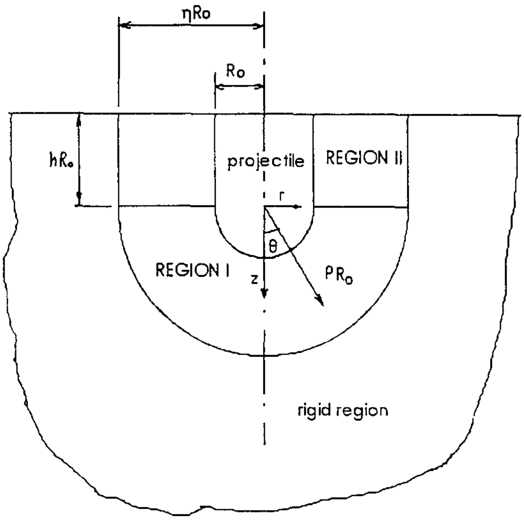

Fig. 2. A schematic sketch of the deforming target regions during stage 2 of the penetration process.

circumferential directions and region II wherein the particles are moving essentially backwards in the axial direction (cf. Fig. 2). We assume that this mode of deformation lasts till the penetration depth equals $2R_0$.

Because of the presumed axisymmetric deformations of the target, we use a spherical coordinate system (ρ, θ, ϕ) with origin at the center of the hemispherical nose of the penetrator to describe the velocity field in region I and a cylindrical coordinate system (r, z) with the same origin to describe the velocity field in region II. The lengths ρ, r and z are scaled by R_0. We note that the penetrator decelerates. Since we will be finding the instantaneous rate of work due to different forces and minimizing the total dissipation rate, the decreasing speed of the coordinate system does not introduce any additional terms in the expressions for $\dot{W}_f$, $\dot{W}_v$, etc. The presumed velocity field in region I should satisfy the following compatibility conditions at the interfaces.

$$
\begin{aligned}
v_\rho^{\mathrm{I}}|_{\rho=\eta} &= 0,\\
v_\rho^{\mathrm{I}}|_{\rho=1} &= V_p\cos\theta,\\
v_\theta^{\mathrm{I}}|_{\rho=1} &= -V_p\sin\theta,\\
v_\theta^{\mathrm{I}}|_{\theta=90^\circ} &= -v_z^{\mathrm{II}}|_{z=0},\\
v_r^{\mathrm{II}}|_{r=1} &= 0,\\
v_r^{\mathrm{II}}|_{r=\eta} &= 0.
\end{aligned}
\tag{15}
$$

Here superscripts I and II signify quantities for regions I and II.

A velocity field that satisfies boundary conditions [eqn (15)] is given by eqn (13) in region I (defined by $1 \leqslant \rho \leqslant \eta$, $0 \leqslant \theta \leqslant \pi/2$) and by

$$v_z = V_p\left[1 - \frac{\eta^3}{(\eta-1)^3}\left(\frac{1}{2r} - \frac{1}{2r^3}\right)\right], \tag{16a}$$

$$v_r = 0, \tag{16b}$$

in region II defined by $1 \leqslant r \leqslant \eta$, $-h \leqslant z \leqslant 0$. This velocity field, shown in Fig. 3, satisfies $\operatorname{div}\mathbf{v} = 0$ and hence the mass density of the target material stays unchanged. $\dot{W}_v$ for region I is given by eqn (14) and for region II,

$$\dot{W}_v = \frac{\pi R_0^3 V_p(\sigma_y)_2}{\sqrt{3}}\frac{h\eta^3}{(\eta-1)^2}f(\eta), \tag{17a}$$

with

$$f(\eta) = \begin{cases} \dfrac{3}{2} - \left(\dfrac{1.5}{\eta^2} + \ln\eta\right), & \eta \leqslant \sqrt{3},\\ \ln\eta + \dfrac{3}{2\eta^2} + \dfrac{3}{2} - \ln 3, & \eta > \sqrt{3}. \end{cases} \tag{17b}$$

Substitution for $\mathbf{v}$ from eqn (13) into the expressions for $\dot{W}_d$ and $\dot{W}_k$ gives

$$\dot{W}_d = 2\pi R_0^3\rho_t\int_{\Omega_1}(\dot{v}_\rho v_\rho + \dot{v}_\theta v_\theta)\rho\,\mathrm{d}\rho\,\mathrm{d}\theta, \tag{18a}$$

$$\dot{W}_k = 2\pi R_0^2\rho_t\int_{\Omega_1}\left[v_\rho^2\frac{\partial v_\rho}{\partial\rho} + v_\rho v_\theta\left(\frac{1}{\rho}\frac{\partial \mathbf{v}_\rho}{\partial\theta} + \frac{\partial v_\theta}{\partial\rho}\right) + \frac{v_\theta^2}{\rho}\frac{\partial v_\theta}{\partial\theta}\right]\rho\,\mathrm{d}\rho\,\mathrm{d}\theta \tag{18b}$$

for region I, and

$$\dot{W}_d = 2\pi R_0^3\dot{V}_p V_p\rho_t h\left[-\frac{1+\eta^2}{2} + \frac{\eta^2(3\eta^2-1)(\eta+1)}{16(\eta-1)^3} + \frac{\eta^6\ln\eta}{4(\eta-1)^4}\right] \tag{18c}$$

$$\dot{W}_k = 0 \tag{18d}$$

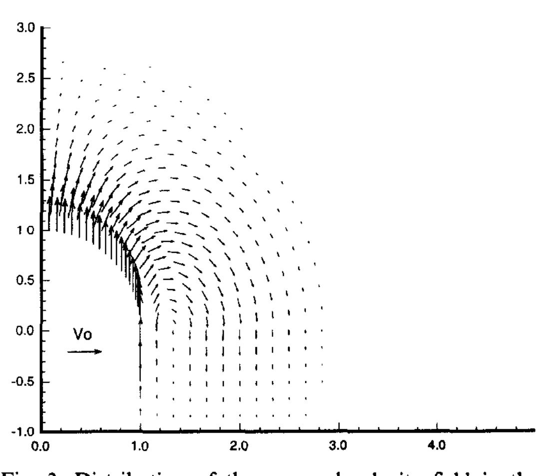

Fig. 3. Distribution of the assumed velocity field in the deforming target region.

for region II. Note that the value of h as a function of time t is determined from the position of the penetrator; the small thickness of the lip region formed is neglected when finding h. Also, V_p and $\dot{V}_p$ equal, respectively, the instantaneous velocity and acceleration of the penetrator.

The boundary conditions [eqn (14)] imply that there is no relative sliding of the target material over the penetrator surface; thus $\dot{W}_s = 0$ for the surfaces $r = 1$ and $\rho = 1$. For the surface $\rho = \eta$ in region I,

$$\dot{W}_s = \frac{\pi R_0^2 V_p (\sigma_y)_I}{4\sqrt{3}} \frac{\eta^2 |\eta - 3|}{(\eta - 1)} \tag{18e}$$

and for the surface $r = \eta$ in region II,

$$\dot{W}_s = \frac{\pi R_0^2 V_p (\sigma_y)_{II}}{\sqrt{3}} \frac{h\eta |\eta - 3|}{(\eta - 1)}. \tag{18f}$$

When the depth of penetration exceeds $2R_0$, i.e. $h > 1$ the velocity field given by eqn (13) needs to be modified since the target material in region II cannot flow backwards freely.

3.3. *Stage* 3. *Tunnel formation*

For penetration depths exceeding $2R_0$, the deforming target region is again divided into regions I and II depicted in Fig. 2. Whereas the velocity field in region I is given by equations (13a, b), that in region II is assumed to be as follows:

$$v_r = 0, \tag{19a}$$

$$v_z = V_p\left(1 + \frac{z}{h}\right)^2 \left[1 - \frac{\eta^3}{2(\eta - 1)^2}\left(\frac{1}{r} - \frac{1}{r^3}\right)\right], \quad -h \leqslant z \leqslant 0. \tag{19b}$$

The target particles can slide on the cylindrical portion of the penetrator. Corresponding to the velocity field given by eqn (19), expressions for $\dot{W}_v$, $\dot{W}_s$, $\dot{W}_f$, $\dot{W}_d$ and $\dot{W}_k$ for region II are given below:

$$\dot{W}_v = \frac{2\sqrt{2}\pi R_0^3 V_p (\sigma_y)_2 h}{3\sqrt{3}} \int_1^\eta \frac{r}{A(r)} \times [(A(r) + C(r))^{3/2} - (C(r))^{3/2}]\, dr, \tag{20a}$$

where

$$A(r) = \frac{\eta^6}{8(\eta - 1)^4}\left(\frac{1}{r^2} - \frac{3}{r^4}\right)^2, \tag{20b}$$

$$C(r) = \frac{4}{h^2} F_r^2, \tag{20c}$$

$$F_r = 1 - \frac{\eta^3}{2(\eta - 1)^2}\left(\frac{1}{r} - \frac{1}{r^3}\right); \tag{20d}$$

$$\dot{W}_s = \frac{\pi R_0^2 V_p (\sigma_y)_{II} h}{3\sqrt{3}} \frac{\eta |\eta - 3|}{(\eta - 1)}, \tag{20e}$$

$$\dot{W}_f = \frac{4\pi R_0^2 V_p \bar{\sigma}_y h \mu}{3\sqrt{3}}, \tag{20f}$$

$$\dot{W}_d = 2\pi R_0^3 \dot{V}_p V_p \rho_t h \int_1^\eta \left(\frac{1}{5} - \frac{V_p \Delta t}{3R_0 h} F_r\right) F_r^2 r\, dr, \tag{20g}$$

$$\dot{W}_k = 2\pi R_0^2 V_p^3 \rho_t \int_1^\eta \left(\frac{1}{3} - \frac{4V_p \Delta t}{7R_0 h} F_r\right) F_r^2 r\, dr. \tag{20h}$$

For the velocity field given by eqn (19), div $\mathbf{v} \neq 0$. The change $\Delta\rho$ in the average mass density of the target material in region II from time t to time $(t + \Delta t)$ is given by

$$\Delta\rho = \frac{V_p \Delta t}{R_0 h(\eta^2 - 1) + V_p \Delta t} \rho_t. \tag{21}$$

3.4. *Stage* 4. *Formation and ejection of plug*

Once the front of the plastic zone reaches the rear surface of the target, a spherical bulge begins to form on the rear surface. The target material enclosed in the conical region (see Fig. 4) is assumed to move as a rigid body with the velocity of the projectile and is excluded from the region I when calculating the dissipation rate. The velocity fields in region II and the remainder of region I are taken to be the same as those in stage 3. The bulge at the back surface grows as the penetrator advances to the rear of the target. When the diameter L (cf. Fig. 4) of the bulge equals $2R_0$, the target material enclosed in the cylinder ahead of the penetrator is assumed to eject out of the target with the velocity

$$v_{exit} = \frac{V_p^f m_p + m_t V_t^f}{m_t + m_p} \tag{22}$$

where V_p^f is the speed of the penetrator at the instant L equals $2R_0$, m_t is the mass of the target material in the shaded cylindrical region in Fig. 4 and V_t^f its

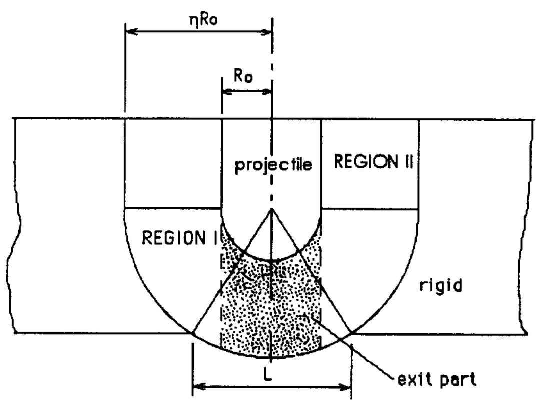

Fig. 4. Plug formation and ejection during stage 4 of the penetration process.

average axial speed at this instant. Equation (22) is obtained by using the conservation of linear momentum. Ideally, one should base the formation of the plug on a certain material property such as the fracture toughness attaining a critical value. However, it is not clear how to do so in the present problem.

We note that for very thick targets or low impact speeds, stage 4 may not occur at all. Similarly for very thin targets, stage 2 and/or stage 3 may be absent.

3.5. *Solution procedure*

At each instant of the penetration process, boundaries of regions I and II are obtained by minimizing the dissipation work rate. The deceleration of the penetrator is then computed from eqn (13), the speed of the penetrator is updated, the incremental and thus the total depth of penetration is computed. Once the instantaneous penetrator speed and the boundaries of regions I and II are known, the velocity field throughout the deforming region is known and one can find at every point of the deforming target region the components of the strain-rate tensor, the effective strain-rate and hence the effective strain, and the incremental displacements of target particles. Thus the time-history of the penetrator speed, the depth of penetration and the deformed shape of the target at any time can be determined. Also time-histories of the effective strain at numerous material points are computed and stored; the values of the effective plastic strain at other material points can be obtained by using an interpolation technique. Figure 5 depicts the deformed target region at some time during the penetration process. The grid lines were initially horizontal and vertical and were uniformly spaced. The shapes of the deformed quadrilateral regions indicate the amount of deformation caused there. It is evident that severe deformations occur near the target/penetrator interface and the most intensely deformed region is not near the stagnation point but adjoins the point on the penetrator/target interface

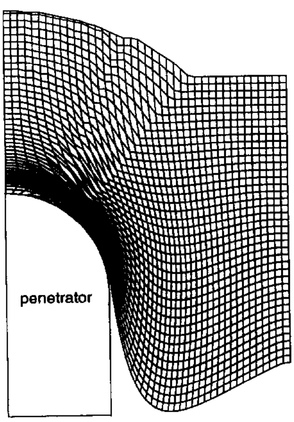

Fig. 5. Deformed shape of the target at some time during the penetration process.

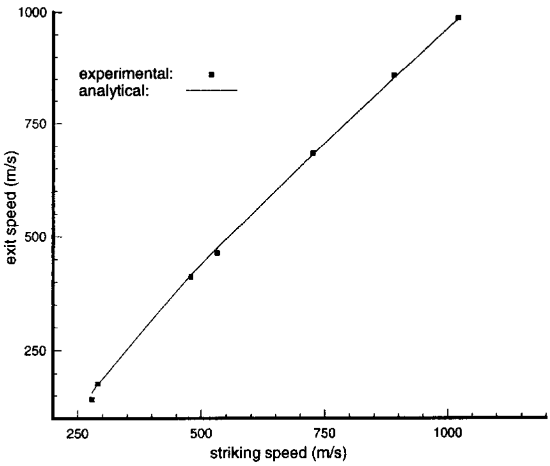

Fig. 6. A comparison of the computed exit speed with the test values.

whose angular coordinate equals nearly 45°. Note that the grid lines are for reference only and play no role in the solution of the problem. Also the location of the severely deformed target material on the penetrator nose will change with time.

4. COMPARISON OF COMPUTED AND TEST RESULTS

We use the aforestated technique to simulate the impact experiments of Forrestal and Luk [12]. The flow stress of target material is assumed to be described by

$$\sigma_y = (350 + 100\epsilon_{\text{eff}})\ \text{MPa}$$

and the penetrator is regarded as rigid. The values of other material and geometric parameters used to compute numerical results are given below:

$$\rho_t = 2660\ \text{kg/m}^3, \quad m_p = 25.8\ \text{g}, \quad \mu = 0.07,$$

$$R_0 = 4.16\ \text{mm},$$

$$\text{Thickness of the target plate} = 1.27\ \text{cm}.$$

Since the target thickness equals $3.05R_0$ stage 3 is of very little duration. As shown in Fig. 6, the computed exit speed of the penetrator matches very well with the test values. In order to compute these results, the time step size used was 0.1 μs. As will be shown below, the precise value of the coefficient of friction between 0.05 and 0.2 has minimal effect on the computed penetration depth and the resisting force experienced by the penetrator.

Tests conducted by Forrestal *et al.* [13] involving deep penetration of steel rods into thick aluminum targets were also simulated. Depending upon the radius and mass of the penetrators, the tests can be divided into three groups:

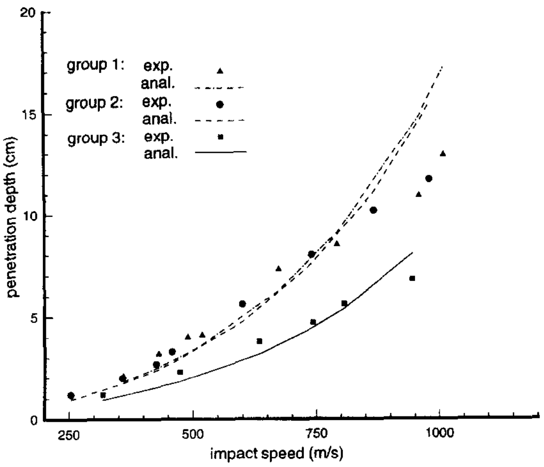

Fig. 7. A comparison of the computed depth of penetration with the test values.

- group 1: $R_0 = 3.555$ mm, $m_p = 23.4$ g,
- group 2: $R_0 = 2.54$ mm, $m_p = 11.8$ g,
- group 3: $R_0 = 3.555$ mm, $m_p = 12.1$ g.

In each case the mechanical response of the target material is modeled by

$$\sigma_y = (290 + 100\epsilon_{eff})\ \text{MPa},$$

the mass density of the target material was set equal to 2710 kg m^{-3} and the coefficient of friction at the sliding surfaces was set equal to 0.07. In computing numerical results, the time step size was taken to be 0.1 μs. As illustrated in Fig. 7, the computed penetration depths match well with the test values. Chen and Batra [11] simulated these tests by numerically solving the complete set of governing equations and used an adaptive mesh refinement technique. Results computed herein match well with those of Chen and Batra. A difference between their work and the present work is that they allowed for the sliding of the target material on the penetrator nose surface but we did not. In each case the computed penetration depth exceeded the test values at high impact speeds. Some of the reasons for this difference are: (i) frictional force at the target/penetrator interface; (ii) blunting of the penetrator nose at high impact speeds; (iii) dependence of the material properties of the target upon the temperature rise; and (iv) different values of the target thickness relative to the penetrator length. In the tests and thus in our simulations, the target length equalled four or five times the penetration depth for low impact speeds and only twice the penetration depth for higher speeds. Thus, support conditions at the back surface may affect the penetration depth more at high impact speeds than at low impact speeds. We took the back surface to be traction free in every case.

In order to delineate the effect of the coefficient of friction μ on the solution of the problem, we have plotted in Fig. 8 for different values of μ the time-history of the penetrator speed and the resisting force experienced by the penetrator for a penetrator from group 3 whose initial impact speed equalled 806 m s^{-1}. It is clear that the value of μ does not affect much the resisting force experienced by the pentrator and therefore the penetration depth. This could partly be due to the frictional force acting on the cylindrical portion of the target/penetrator interface only during stage 3 of the penetration process. Chen and Batra [11], who accounted for the frictional force on all of the target/penetrator interface, found that the values of μ between 0 and 0.12 affected noticeably the penetration depth but higher values of μ did not change appreciably the computed values of penetration depth. The kink in the time-history of the resisting force corresponds to the change in the deformation pattern from stage 1 to stage 2. The resisting force curve agrees both qualitatively and

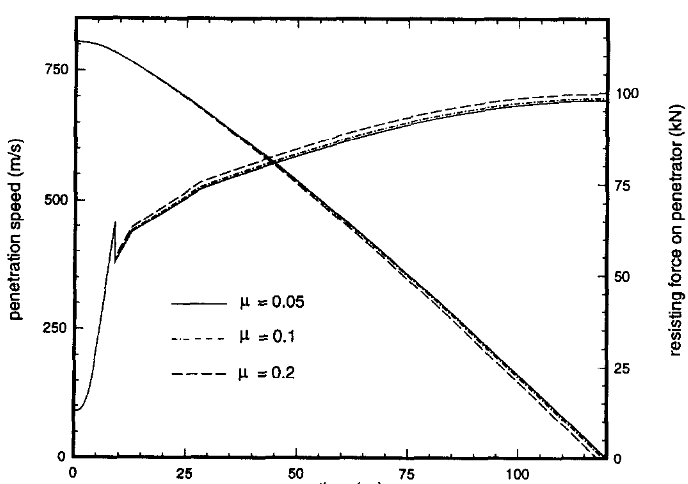

Fig. 8. Effect of the values of the coefficient of friction upon the time-histories of the penetration speed and the resisting force experienced by the penetrator.

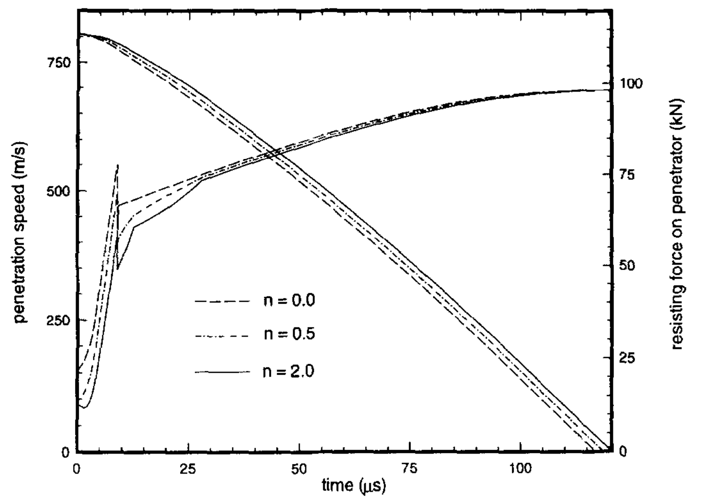

Fig. 9. Effect of the value of the strain-hardening exponent upon the time-histories of the penetration speed and the resisting force experienced by the penetrator.

quantitatively with that of Chen and Batra [11], signifying thereby that the proposed engineering model yields good results.

In an attempt to assess the effect of the value of the strain-hardening exponent n in eqn (3) on the solution of the problem, we modeled the flow stress of the target material by

$$\sigma_y = (290 + 100(\epsilon_{\text{eff}})^n)\,\text{MPa}.$$

Figure 9 depicts the time-histories of the resisting force experienced by the penetrator and the penetrator speed for $n = 0$, 0.5 and 2.0. Higher values of n enhance the resisting force acting on the penetrator and hence decelerate it more. However, for $t \geqslant 40\ \mu$s, the resisting force acting on the penetrator, and thus the deceleration of the penetrator, is unaffected by the value of n.

5. CONCLUSIONS

We have developed a four stage engineering model of target penetration/perforation by a hemispherical-nosed rigid cylindrical penetrator. During each stage of penetration, a kinematically admissible velocity field involving one or more unknown parameters is presumed. The values of unknown parameters are first determined by minimizing the dissipation work-rate; then the speed of the penetrator, the deformed shape of the target, and the deceleration of the penetrator are updated after each increment in time. A model for the formation and ejection of the plug is proposed and used to study the perforation of aluminum plates by steel cylindrical rods which are assumed to be rigid. The computed exit speeds of the projectiles for perforated plates and the computed penetration depths for thick targets are found to match very well with the corresponding test values. Thus the simple model proposed herein yields very good values of the penetration depths and the exit speeds of the projectile.

Acknowledgement—This work was supported by the U.S. Army Research Office grants DAAL03-92G-0315 to the University of Missouri-Rolla and DAAH04-95-1-0042 to the Virginia Polytechnic Institute and State University.

REFERENCES

1. M. Ravid and S. R. Bodner, *Int. J. Engng Sci.* **21**, 577 (1983).
2. R. C. Batra and X. Chen, *Int. J. Engng Sci.* **28**, 1347 (1990).
3. G. Birkhoff, D. P. Mcdougall, E. M. Pugh and G. Taylor, *Proc. Phys. Soc. Lond.* **57**, 147 (1945).
4. D. C. Pack and W. M. Evans, *Proc. Phys. Soc. Lond.* **B64**, 298 (1951).
5. W. A. Allen and J. W. Rogers, *J. Franklin Inst.* **272**, 275 (1961).
6. V. P. Alekseevskii, *Combust. Explos. Shock Waves* **2**, 63 (1966).
7. A. Tate, *J. Mech. Phys. Solids* **15**, 386 (1967).
8. A. Tate, *J. Mech. Phys. Solids* **17**, 141 (1969).
9. J. Martin, *Int. J. Solids Struct.* **8**, 1185 (1972).
10. R. C. Batra and X. Chen, *Acta Mech.* **106**, 87 (1994).
11. X. Chen and R. C. Batra, *Comput. Struct.* **54**, 655 (1995).
12. M. Forrestal and V. Luk, *Mech. Mater.* **10**, 95 (1990).
13. M. Forrestal, N. Brar and V. Luk, *J. appl. Mech.* **58**, 7 (1991).